Published online 2 March 2016

Nucleic Acids Research, 2016, Vol. 44, No. 10 ***e94***
doi: 10.1093/nar/gkw117

Engineering a ribozyme cleavage-induced split fluorescent aptamer complementation assay

Simon Ausländer[1,†], David Fuchs[1,†], Samuel Hürlemann[1], David Ausländer[1] and Martin Fussenegger[1,2,*]

[1]Department of Biosystems Science and Engineering, ETH Zurich, Mattenstrasse 26, CH–4058 Basel, Switzerland and [2]Faculty of Science, University of Basel, Mattenstrasse 26, CH-4058 Basel, Switzerland

Received October 15, 2015; Revised February 02, 2016; Accepted February 16, 2016

ABSTRACT

Hammerhead ribozymes are self-cleaving RNA molecules capable of regulating gene expression in living cells. Their cleavage performance is strongly influenced by intra-molecular loop–loop interactions, a feature not readily accessible through modern prediction algorithms. Ribozyme engineering and efficient implementation of ribozyme-based genetic switches requires detailed knowledge of individual self-cleavage performances. By rational design, we devised fluorescent aptamer-ribozyme RNA architectures that allow for the real-time measurement of ribozyme self-cleavage activity *in vitro*. The engineered nucleic acid molecules implement a split Spinach aptamer sequence that is made accessible for strand displacement upon ribozyme self-cleavage, thereby complementing the fluorescent Spinach aptamer. This fully RNA-based ribozyme performance assay correlates ribozyme cleavage activity with Spinach fluorescence to provide a rapid and straightforward technology for the validation of loop–loop interactions in hammerhead ribozymes.

INTRODUCTION

Ribonucleic acid (RNA) molecules are highly versatile macromolecules that perform a plethora of functions in living cells, such as transmitting and converting genetic information, regulating gene expression, organizing complex riboprotein-based molecular machines and performing enzymatic activities (1). An increasing number of synthetic RNAs with novel functionalities, such as ligand-binding RNA structures (aptamers) (2) or self-replicating RNA enzymes (3), add to their natural diversity. The predictable design of RNA–RNA interactions via simple Watson-Crick base-pairing rules enables the programmable strand displacement that is essential for the design of synthetic RNA circuits (4,5) or the engineering of riboregulators that control bacterial gene expression (6,7). Additionally, functional RNA modules (e.g. aptamers) fold into distinct secondary or tertiary structures that can be interconnected to provide novel biomolecular devices, such as ligand-responsive gene regulation systems (8–10).

Ribozymes have the ability to (self-)cleave RNA and are therefore valuable building blocks for RNA engineering (11). For example, hammerhead ribozymes (HHRs) are small RNA modules that can be artificially integrated into bacterial (12), yeast (13,14) and mammalian (15) mRNAs to control mRNA stability. Moreover, combinations of HHRs with RNA aptamers render their self-cleavage activity ligand dependent and are thus useful tools for programmable gene control (11). HHRs fold into a distinct tertiary structure composed of a three-way junction where stem loops I/II form a specific interaction required for efficient self-cleavage (16). Although the catalytic region is highly conserved, the nucleotide composition of the stem loops differs within individual HHR species, indicating that there are many methods to form the required loop–loop interaction that facilitates folding into an active ribozyme conformation (17).

Fluorescent RNA aptamers exhibit fluorescence upon binding specific ligands and are useful readout modules for engineered RNA-based devices (18,19). For example, the RNA aptamer Spinach specifically binds to the fluorophore (Z)-4-(3,5-difluoro-4-hydroxybenzylidene)-1,2-dimethyl-1H-imidazol-5(4H)-one (DFHBI), resulting in green fluorescence (19). Fluorescent aptamers are promising tools for imaging RNAs in living cells (20). When re-engineered or combined with other functional RNA parts, the Spinach aptamer can also serve as a fully RNA-based readout module to detect metabolites or oligonucleotides (4,5,21,22). Dividing the Spinach aptamer into two separate RNA strands enables DNA-programmable aptamer reconstitution and monitoring of DICER processing *in vitro* (23).

*To whom correspondence should be addressed. Tel: +41 61 387 31 60; Fax: +41 61 387 39 88; Email: fussenegger@bsse.ethz.ch
†These authors contributed equally to the paper as first authors.

Table 1. Plasmids designed and used in this study

Name	Elements	Description	Reference
pDF101	P_{T7}-SpA_L-$sTRSV_{ac}$	ODF76 was PCR-amplified with ODF77 and ODF81, restricted with *Eco*RI and *Xba*I and ligated into pUC57 (*Eco*RI/*Xba*I).	This work
pDF102	P_{T7}-SpA_L-$sTRSV_{inac}$	ODF76 was PCR-amplified with ODF78 and ODF81, restricted with *Eco*RI and *Xba*I and ligated into pUC57 (*Eco*RI/*Xba*I).	This work
pDF103	P_{T7}-SpA_M-$sTRSV_{ac}$	ODF76 was PCR-amplified with ODF79 and ODF81, restricted with *Eco*RI and *Xba*I and ligated into pUC57 (*Eco*RI/*Xba*I).	This work
pDF104	P_{T7}-SpA_M-$sTRSV_{inac}$	ODF76 was PCR-amplified with ODF80 and ODF81, restricted with *Eco*RI and *Xba*I and ligated into pUC57 (*Eco*RI/*Xba*I).	This work
pDF105	P_{T7}-SpA_H-$sTRSV_{ac}$	ODF76 was PCR-amplified with ODF89 and ODF81, restricted with *Eco*RI and *Xba*I and ligated into pUC57 (*Eco*RI/*Xba*I).	This work
pDF106	P_{T7}-SpA_H-$sTRSV_{inac}$	ODF76 was PCR-amplified with ODF90 and ODF81, restricted with *Eco*RI and *Xba*I and ligated into pUC57 (*Eco*RI/*Xba*I).	This work
pDF107	P_{T7}-SpFL	ODF86 and ODF81 were annealed, filled in by PCR, restricted with *Eco*RI and *Xba*I and ligated into pUC57 (*Eco*RI/*Xba*I).	This work
pDF109	P_{T7}-SpB	ODF88 and ODF81 were annealed, filled in by PCR, restricted with *Eco*RI and *Xba*I and ligated into pUC57 (*Eco*RI/*Xba*I).	This work
pDF145	P_{T7}-SpA_H-$Env140_{ac}$	ODF150 and ODF151 were annealed, filled in by PCR, and PCR-amplified with ODF81 and ODF167, restricted with *Eco*RI and *Xba*I and ligated into pUC57 (*Eco*RI/*Xba*I).	This work
pDF146	P_{T7}-SpA_H-$Env140_{inac}$	ODF152 and ODF153 were annealed, filled in by PCR, PCR-amplified with ODF81 and ODF168, restricted with *Eco*RI and *Xba*I and ligated into pUC57 (*Eco*RI/*Xba*I).	This work
pDF148	P_{T7}-SpA_H-Env140-$C3_{ac}$	ODF154 and ODF155 were annealed, filled in by PCR, PCR-amplified with ODF81 and ODF167, restricted with *Eco*RI and *Xba*I and ligated into pUC57 (*Eco*RI/*Xba*I).	This work
pDF151	P_{T7}-SpA_H-Env140-$H1_{ac}$	ODF156 and ODF157 were annealed, filled in by PCR, PCR-amplified with ODF81 and ODF167, restricted with *Eco*RI and *Xba*I and ligated into pUC57 (*Eco*RI/*Xba*I).	This work
pDF168	P_{T7}-SpA_H-sTRSV-$L1.3_{ac}$	ODF185 was PCR-amplified with ODF89 and ODF81, restricted with *Eco*RI and *Xba*I and ligated into pUC57 (*Eco*RI/*Xba*I).	This work
pDF169	P_{T7}-SpA_H-sTRSV-$L1.5_{ac}$	ODF93 was PCR-amplified with ODF89 and ODF81, restricted with *Eco*RI and *Xba*I and ligated into pUC57 (*Eco*RI/*Xba*I).	This work
pDF179	P_{T7}-SpA_H-sTRSV-$L1.6_{ac}$	ODF184 was PCR-amplified with ODF89 and ODF81, restricted with *Eco*RI and *Xba*I and ligated into pUC57 (*Eco*RI/*Xba*I).	This work

Abbreviations: Env140: engineered hammerhead ribozyme derived from environmental samples; **ODFn:** DNA oligonucleotide number n; **P_{T7}:** Promoter recognized by phage T7 RNA-polymerase; **$SpA_{L/M/H}$:** Split Spinach aptamer 5′ part with low (L), medium (M) or high (H) base-pairing strength; **SpB**: Split Spinach aptamer 3′ part; **SpFL:** Full-length Spinach aptamer; **sTSRV**: engineered hammerhead ribozyme derived from the natural ribozyme from the satellite RNA of the tobacco ringspot virus.

Table 2. DNA oligonucleotides designed and used in this study

Name	Sequence (5′-3′)
ODF42	TCCTCACGGACTCGTCAGCCC
ODF76	CGTCCTCACGGACTCGTCAGCCCGGAAAGCACATCCGGGGACGCACTGGACCCGTCCTTCTCCCCTATAGTGAGTCGTATTAGAATTCGCTG
ODF77	ATGCTCTAGATGGCCAATACGTTTCGTCCTCACGGACTCGTCAG
ODF78	ATGCTCTAGATGGCCAATACGTCTCGTCCTCACGGACTCGTCAG
ODF79	ATGCTCTAGATGGCCAATGCGTTTCGTCCTCACGGACTCGTCAG
ODF80	ATGCTCTAGATGGCCAATGCGTCTCGTCCTCACGGACTCGTCAG
ODF81	CAGCGAATTCTAATACGACTCACTATAGG
ODF89	ATGCTCTAGATGGCCAGTGCGTTTCGTCCTCACGGACTCGTCAG
ODF93	CGTCCTCACGGACTCGTCAGCCCGGAAACCACATCCGGGGACGCACTGGACCCGTCCTTCTCCCCTATAGTGAGTCGTATTAGAATTCGCTG
ODF90	ATGCTCTAGATGGCCAGTGCGTCTCGTCCTCACGGACTCGTCAG
ODF98	GAAGCATTTATCAGGGTTATTGTCTCATGAGC
ODF99	CCTGCGTTATCCCCTGATTCTGTGGATAACC
ODF150	TAATACGACTCACTATAGGGGAGAAGGACGGGTCCAGTGCGTCCGGGGGCTGGACCGCCCCCGCTGACGAGGCC
ODF151	GGATGATCTAGATGGCCAATGCGTTTCGGCCCTCCGCGGGCCTCGTCAGCGGGGCGGTCCA
ODF152	TAATACGACTCACTATAGGGGAGAAGGACGGGTCCAGTGCGTCCGGGGCTGAATCGCCCCGCTGACGAGCCCTG
ODF153	GGATGATCTAGATGGCCAATGCGTTTCGCCCTTTTTCAGGGCTCGTCAGCGGGGCGATTCAG
ODF154	TAATACGACTCACTATAGGGGAGAAGGACGGGTCCAGTGCGTCCGGGGCTCCCCTGCCCCGCTGACGAGC
ODF155	GGATGATCTAGATGGCCAATGCGTTTCGCCCTTTTTCAGGGCTCGTCAGCGGGGCAGGGGAG
ODF156	TAATACGACTCACTATAGGGGAGAAGGACGGGTCCAGTGCGTCCGGGGCTGGACCGCCCCGCTGACGAGCCCTG
ODF157	GGATGATCTAGATGGCCAATGCGTTTCGCCCTTTTTCAGGGCTCGTCAGCGGGGCGGTCCAG
ODF167	GGATGATCTAGATGGCCAGTGCGTTTCG
ODF168	GGATGATCTAGATGGCCAGTGCGTCTCG
ODF170	GCGGGCCTCGTCAGCGGGGCG
ODF171	TCAGGGCTCGTCAGCGGGGCG
ODF172	TCAGGGCTCGTCAGCGGGGCA
ODF184	CGTCCTCACGGACTCGTCAGCCCGGAAGGCACATCCGGGGACGCACTGGACCCGTCCTTCTCCCCTATAGTGAGTCGTATTAGAATTCGCTG
ODF185	CGTCCTCACGGACTCGTCAGCCCGGAAAGCCCATCCGGGGACGCACTGGACCCGTCCTTCTCCCCTATAGTGAGTCGTATTAGAATTCGCTG

MATERIALS AND METHODS

Plasmid cloning

Table 1 lists all plasmids used in this study and provides detailed information about their construction. All relevant genetic components have been confirmed by sequencing (Microsynth, Balgach, Switzerland). Table 2 lists all DNA oligonucleotide sequences used for the construction of the plasmids.

In vitro transcription

DNA templates of HHR variants were generated by PCR-mediated amplification from a pUC57 backbone (Piscataway NJ/US) using ODF98 and ODF99 (see Table 2) and subsequent blunt-end restriction. Blunt-end restriction using *Msc*I (New England Biolabs, Ipswich MA/US) resulted in a dsDNA fragment containing the promoter sequence for phage T7 RNA polymerase, the HHR-coding sequence and a 578-bp untranscribed region upstream of the promoter. This template was transcribed *in vitro* using the HiScribe T7

High Yield RNA Synthesis Kit (NEB, Ipswich MA). The composition of the reaction mix differed from the manufacturers suggestions by using 0.5x NEB transcription buffer and adding 1.25 mM EDTA as well as addition of 60 μM of a DNA 21-mer (see Table 2) reverse complementary to the HHR catalytic core resulting in an optimized protocol with increased yield of *cis*-cleaving full-length HHRs. *In vitro* transcription reactions were terminated after 5 h at 37°C with one volume of stopping solution (80% v/v formamide, 10% v/v 50 mM EDTA pH 8.0, 10% v/v glycerol, 4°C). Samples were kept on ice until purification. Supplementary Table S1 lists all RNA oligonucleotides produced in this study.

RNA purification

In vitro-transcribed RNAs (for full sequences see Supplementary Table S1) were purified by denaturing polyacrylamide gel electrophoresis on a 10% gel containing 8 M urea at 55°C buffer temperature and an electric field strength of 12 V/cm. Individual RNA bands were visualized by UV-shadowing (excitation wavelength 254 nm), excised from the gel, crushed and eluted into TE buffer (Tris 10 mM pH 7.0, EDTA 1 mM) overnight at 4°C. The resulting RNA solutions were filtered through glass wool and concentrated by ethanol/sodium acetate precipitation. Resulting pure RNA in 1x TE was quantified on a Nanodrop spectrometer (NanoDrop products, Wilmington, DEL/US), diluted to a working stock concentration of 5 μM with ice-cold 1x TE and stored in aliquots at −20°C.

Fluorescence microplate-reader measurements

Cleavage-induced split Spinach fluorescence was measured using a Tecan Infinite M1000 spectrofluorometer (Tecan Group Ltd., Männedorf, Switzerland). Using an excitation/emission wavelength scan, we determined the optimal parameters to quantify Spinach fluorescence (Supplementary Figure S1). Individual reactions were assembled on a black 348-well plate with optically clear bottom (Greiner Bio-One, Frickenhausen, Germany) according to the following specifications. One microlitre of 5 μM Spinach aptamer (SpFL or SpA) or ribozyme RNA was mixed with 9 μl Spinach buffer before starting the measurement. Spinach buffer is based on TNaK buffer with $MgCl_2$ (20 mM Tris, 140 mM NaCl, 100 mM KCl, 0.5 mM $MgCl_2$, pH 7.5) containing 20 μM DFHBI-1T fluorophore (Lucerna Inc., New York, NY/US) and 0.5 μM SpB RNA. The reaction plate was sealed with MicroAmp Optical Adhesive Film (ThermoFisher Scientific, Paisley, UK), and black tape to prevent sample evaporation and background fluorescence. Spinach fluorescence intensity was recorded using the following parameters (interval: 15 s, total duration: 3 h, excitation: 484 ± 5 nm, emission: 508 ± 5 nm, temperature: 30°C, flashes: 25 (400 Hz), gain: 125, integration time: 20 μs). Values of kobs and plateau were obtained by fitting the fluorescence versus time data directly to first-order kinetics using GraphPad Prism 6 (GraphPad Software, CA, USA): $Y_t = Y0 + (Y - Y0) * (1–\exp(–k*t))$, where k = kobs, Y0 = y intercept and Y = plateau.

RESULTS AND DISCUSSION

Split Spinach aptamer is functional

Based on the Spinach aptamer crystal structure (24,25), we engineered and produced a minimalized full-length Spinach aptamer version (SpFL) that is similar to the recently reported 5 bp P1 stem mutant (Figure 1A) (24). SpFL exhibited increased fluorescence levels in TNaK buffer compared with HEPES buffer (Supplementary Figure S2). We further investigated the influence of different magnesium and potassium ion concentrations on SpFL fluorescence in a TNaK-based buffer and revealed that SpFL is fluorescent at physiological magnesium concentrations (0.2–1 mM Mg^{2+}) (Supplementary Figure S3). Even when divided into two parts (SpA and SpB), we observed functional Spinach aptamer reconstitution and fluorescence, resulting in a split Spinach aptamer system similar to that by Rogers et al. (23) (Figure 1A–C). The concentration of SpB was kept constant (2 μM) while we added different concentrations of SpA (0–2 μM). This experiment yielded a linear increase in fluorescence intensity with increasing concentrations of SpA in a dose-dependent manner (Figure 1D).

Design and characterization of the ribozyme-Spinach fusion RNA

We wanted to assess whether we could apply the split Spinach aptamer system as an output module for the development of an HHR performance assay to monitor HHR self-cleavage activity *in vitro*. By rational design, we engineered an HHR-SpA scaffold consisting of a conserved catalytic core and a stem III module with a 5′-connected split SpA component and a variable region consisting of stem loops I/II that determine the ribozyme cleavage activity (Figure 2A). We designed the stem III module to form a stable stem structure to block accessibility to the second split aptamer component SpB and prevent split Spinach reconstitution (Figure 2A and B). We assumed that SpB would only be able to perform a strand-displacement reaction upon ribozyme self-cleavage, thus resulting in reconstitution of the functional Spinach aptamer (Figure 2B). Thus, accessibility of SpA as well as Spinach aptamer fluorescence depends on the self-cleavage activity of the HHR. The thermodynamic stability of stem III is a key parameter for the strand-displacement reaction. To validate the functionality of the ribozyme performance assay, we connected engineered stem loops I/II (see Figure 2C) of the well-characterized sTRSV HHR to our HHR-SpA scaffold. We designed and produced three $sTRSV_{ac/inac}$-SpA variants that differed in their predicted stem III thermodynamic stability (low (SpA_L), medium (SpA_M) and high (SpA_H)) (Figure 2D). For each variant, a point mutation (A14G according to the hammerhead nomenclature (26)) was introduced that completely abolished HHR self-cleavage activity and served as a non-cleaving control (Figure 2A). We performed the assay in 384-well plates using low volumes (10 μl) and 500 nM final RNA concentrations. We then measured real-time fluorescence intensity using a standard fluorescence plate reader. The addition of magnesium-containing TNaK buffer initiated the ribozyme self-cleavage reaction, and fluorescence strongly increased for all three active $sTRSV_{ac}$-

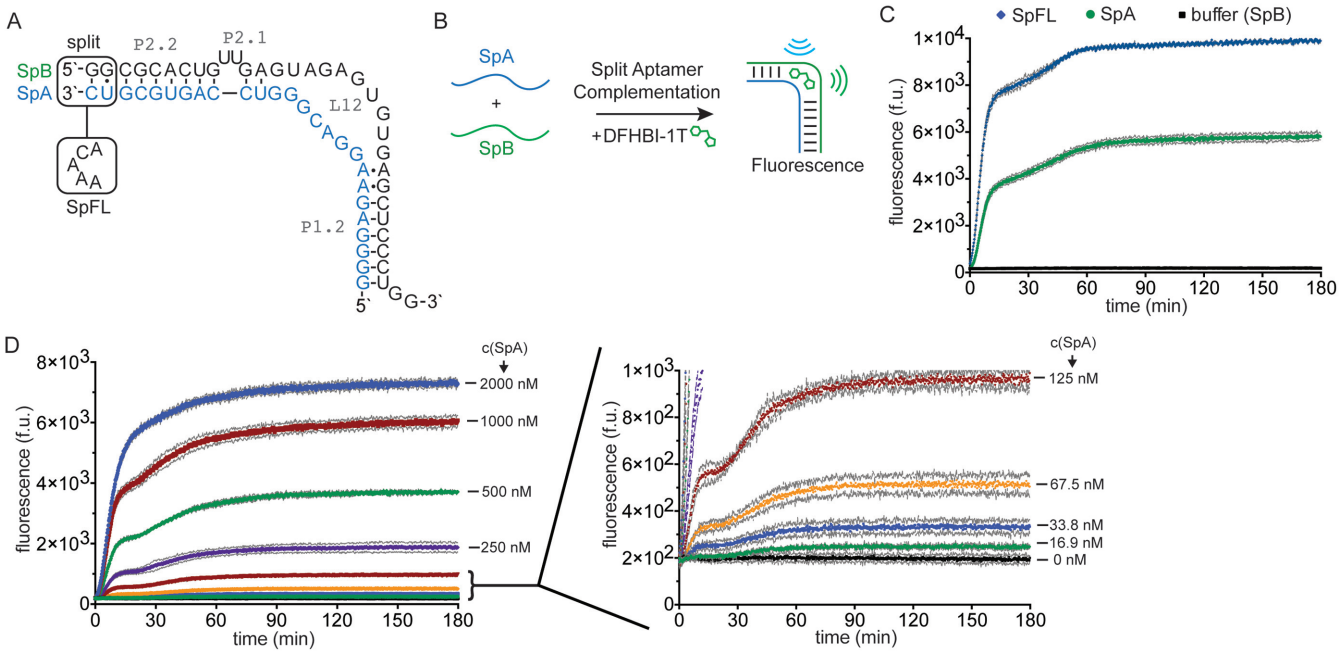

Figure 1. Design and validation of the split Spinach aptamer system. (**A**) Spinach fluorescent aptamer sequence. For the split system, the Spinach aptamer SpFL is divided at the loop structure into two parts resulting in SpA and SpB. (**B**) Working model of the split Spinach aptamer system. SpA and SpB assemble to a functional Spinach aptamer, which binds to the fluorophore DFHBI-1T and emits green fluorescence. (**C**) Fluorescence intensities of 500 nM full-length (blue) and 500 nM split (green) Spinach aptamers. SpA and SpB reconstitute a functional Spinach aptamer (green). (**D**) SpB concentration is kept constant at 2 μM, while SpA is added in different concentrations (0, 1.9, 3.9, 7.8, 15.6, 31.3, 62.5, 125, 250, 500, 1000, 2000 nM). Background fluorescence levels of buffer containing 2 μM SpB are shown in black. Data are mean ± S.D. of a triplicate experiment.

$SpA_{H/M/L}$ variants. Only the inactive variant $sTRSV_{inac}$-SpA_H remained at buffer background levels (Figure 2E–G). However, the increase in fluorescence levels of the inactive variants $sTRSV_{inac}$-$SpA_{M/L}$ featuring reduced stem III stabilities indicated a strand-displacement reaction and split Spinach reconstitution in the absence of ribozyme cleavage. We concluded that the designed HHR-SpA scaffold with a strong stem III (SpA_H) is the most suitable for the HHR performance assay because this design allows clear discrimination of the fluorescence levels of inactive and active ribozymes.

The assay can be used to measure different ribozyme performances

To validate whether the assay may also be used to measure differences in ribozyme cleavage rates of variants with different tertiary loop–loop interactions, we further tested other HHR processing modules with established ribozyme cleavage activities. Compared with sTSRV, the Env140 HHR forms a different tertiary interaction; however, it exhibits a similar cleavage activity in mammalian cells (27). We recently produced a random library of $Env140_{ac}$ derivatives with an engineered protein-binding aptamer in stem loop II that differed in their stem loop I nucleotide composition and self-cleavage activities (Figure 3A) (27). We chose the active and inactive version of the parental $Env140_{ac/inac}$ as well as two active variants of the library with medium ($Env140\text{-}C3_{ac}$) and low ($Env140\text{-}H1_{ac}$) ribozyme performances. The ribozymes were connected to the SpA_H output module to prepare them for the ribozyme performance assay. We monitored the real-time fluorescence of the engineered HHR variants using the established assay (Figure 3B). As expected, the inactive $Env140_{inac}$ HHR maintained background fluorescence while all active $Env140_{ac}$ variants demonstrated an increase in fluorescence levels (Figure 3B). In accordance with the SpA titration experiment (see Figure 1D), the measured fluorescence curve progression differed depending on the ribozyme self-cleavage performance, which controls the amount of ribozyme-liberated SpA. We have quantified the fluorescence curves which resulted in distinct rate constants specific for each ribozyme (Table 3). $Env140_{ac}$-SpA_H exhibited the steepest fluorescence increase as well as the highest fluorescent intensity followed by the medium- and low-performing HHRs $Env140\text{-}C3_{ac}$-SpA_H and $Env140\text{-}H1_{ac}$-SpA_H, respectively (Figure 3B, Table 3). Notably, the *in vitro* measured ribozyme performance ranking compares with the published gene expression data measured in mammalian cells (27). Khvorova et al. (16) have produced a collection of sTRSV HHR mutants to investigate the impact of loop–loop interactions on the ribozyme's self-cleavage activity (16). We have selected representative high- (1.5), medium- (1.3) and low- (1.6) performing mutant ribozymes of this collection and connected them to the SpA_H output module for analysis using the ribozyme performance assay (Figure 3C). Quantification of the corresponding fluorescence curves resulted in values (kobs*plateau) that matched the established performance ranking of these ribozymes reported by Khvorova et al. (16) (Figure 3D, Table 3). The rate constants, however, are 10-fold lower compared to the reported ones. We assume that this difference results from the stable SpA_H output module

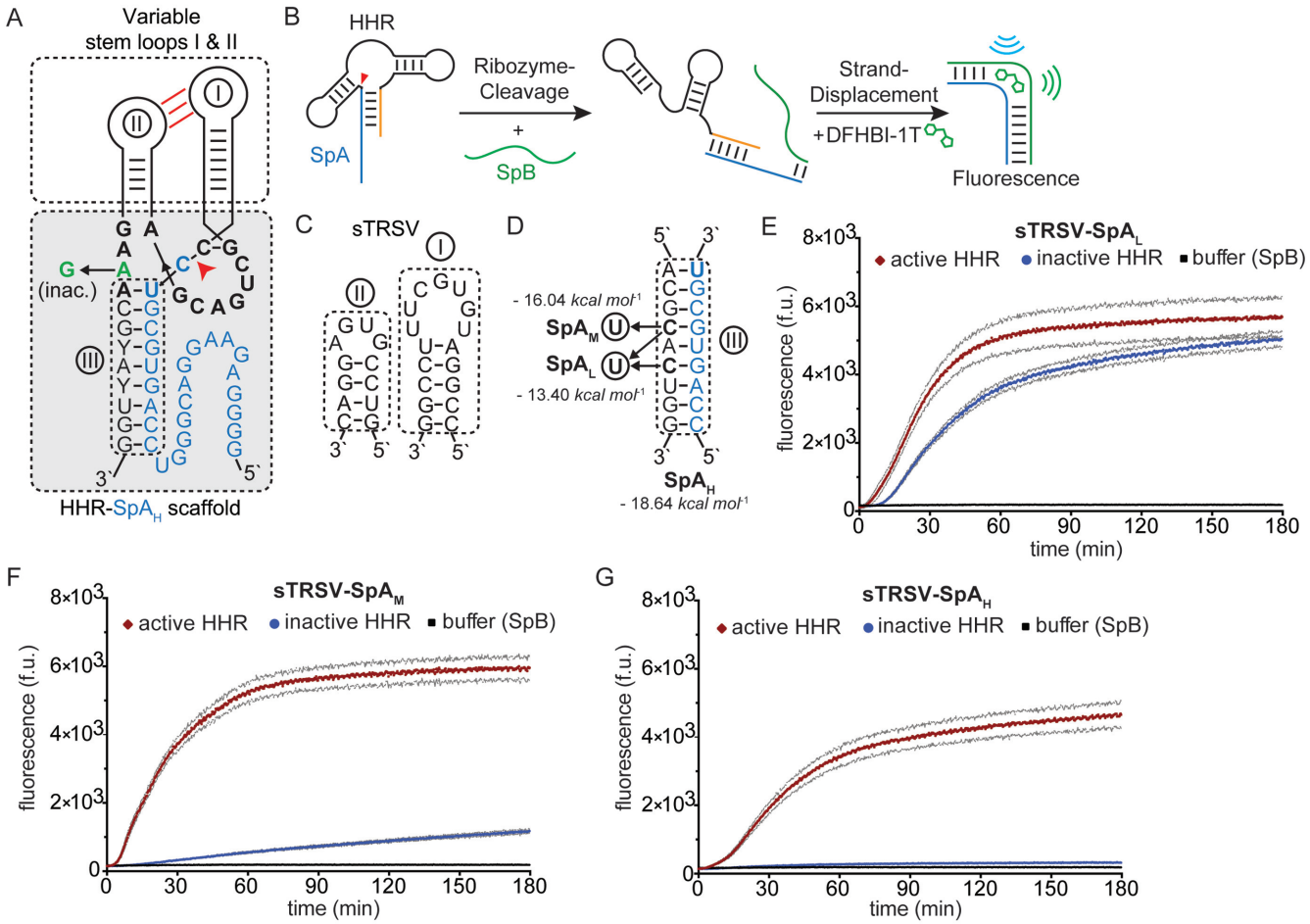

Figure 2. Design and validation of the ribozyme performance assay. (**A**) Nucleotide sequence of the HHR-SpA scaffold. The conserved region is shown as a shaded box and consists of the catalytic core (bold) as well as stem III linked to the 5′-connected split aptamer part SpA (blue). A point mutation A14G (green bold) renders the ribozyme inactive. Variable stem loops can be connected to the HHR-SpA scaffold. (**B**) Working model for the ribozyme performance assay. Ribozyme cleavage releases SpA, which facilitates the strand-displacement reaction required to reconstitute functional fluorescent Spinach aptamer and results in high-level fluorescence. (**C**) Nucleotide sequence of the engineered sTRSV stem loops I and II. (**D**) Design of the stem III variants SpA$_{L/M/H}$ of the HHR-SpA scaffold with their respective Gibbs free energy values ΔG (italics, calculated using the NUPACK web server (31) and the parameter set of Serra & Turner, 1995). (**E–G**) Fluorescence intensities of 500 nM active (red) or inactive (blue) sTRSV-SpA$_L$ (E), sTRSV-SpA$_M$ (F) and sTRSV-SpA$_H$ (G) variants. Background fluorescence of buffer containing 500 nM SpB is shown in black. Data are mean ± S.D. of a triplicate experiment.

that builds a stable 10 base-pair stem III compared to the less stable four base-pair stem III used by Khvorova et al. (16).

In summary, we present a novel assay to monitor ribozyme self-cleavage performances on standard fluorescent plate readers in real-time. Based on an RNA engineering approach, we combined a split-fluorescent aptamer system with HHRs in a manner that couples their self-cleavage activity to aptamer fluorescence. We have used this assay to quantify the self-cleavage activities of established HHRs and measured the same relative ribozyme performances. However, since the assay requires a fixed stem III sequence to connect the SpA split aptamer to the 5′ end of the ribozyme which alters the RNA sequences, the direct comparison of absolute rate constants among different performance-analysis methods needs to be interpreted with care.

Classical approaches to characterize HHR self-cleavage activities employ radioactive labelling (12), artificially modified RNAs (28) or surface plasmon resonance spectroscopy (29). Although each of these methods has advantages, the HHR performance assay is a simple and fully RNA-based assay that can be performed in a high-throughput and low-volume format on standard fluorescent plate readers. The assay may be applied for high-throughput identification of functional loop–loop interactions in HHR libraries consisting of thousands of uncharacterized HHR sequences (17). In addition to the characterization of natural tertiary loop–loop interactions, the assay could also be used to test the self-cleavage performance of engineered, synthetic HHRs. Moreover, the same engineering principle could also be applied to other ribozymes (e.g. the twister ribozyme (30)) to monitor ribozyme cleavage activities. The Spinach aptamer requires stable folding for efficient fluorescence in living cells, which can be achieved by integrating scaffolds,

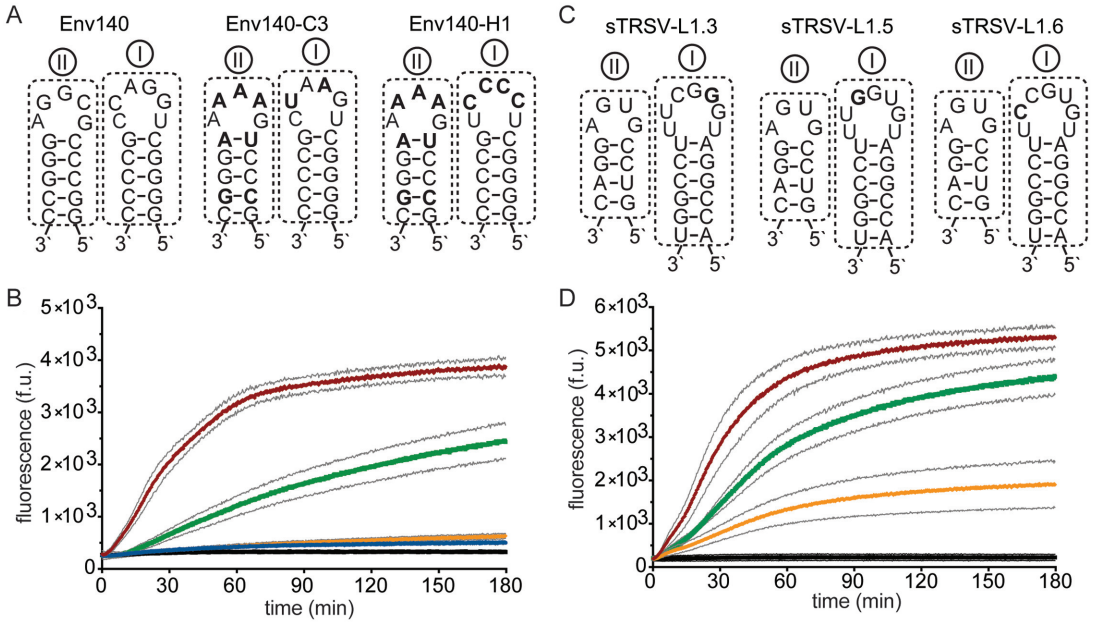

Figure 3. Ribozymes with different self-cleavage activities. (**A**) Nucleotide sequence of the stem loops I/II of Env140, Env140-C3 and Env140-H1 ribozymes. (**B**) Fluorescence intensities of 500 nM active $Env140_{ac}$ (red), active $Env140\text{-}C3_{ac}$ (green), active $Env140\text{-}H1_{ac}$ (yellow) or inactive $Env140_{inac}$ (blue) variants with the HHR-SpA_H scaffold. (**C**) Nucleotide sequence of the stem loops I/II of sTRSV mutant 1.3, 1.5 and 1.6 ribozymes. (**D**) Fluorescence intensities of 500 nM $sTRSV\text{-}1.5_{ac}$ (red), $sTRSV\text{-}1.3_{ac}$ (green) or $sTRSV\text{-}1.6_{ac}$ (yellow) variants with the HHR-SpA_H scaffold. Background fluorescence of buffer containing 500 nM SpB is shown in black. Data are mean ± S.D. of three independent experiments performed in duplicates.

Table 3. Quantification of ribozyme self-cleavage activities

Ribozyme	Kobs [min^{-1}]	Plateau [f.u.]	Kobs*Plateau [f.u./min]	R^2
sTRSV wildtype[a]	0.0216 +/− 0.0002	4522.549 +/− 11.685	97.687	0.99
sTRSV-1.3[b]	0.0126 +/− 0.0002	4391.403 +/− 23.690	55.770	0.95
sTRSV-1.5[b]	0.0273 +/− 0.0002	4642.491 +/− 9.623	126.740	0.94
sTRSV-1.6[b]	0.0176 +/− 0.0002	1026.779 +/− 3.414	18.071	0.95
Env140 wildtype[c]	0.0264 +/− 0.0002	3556.032 +/− 4.982	93.879	0.99
Env140-C3[c]	0.0059 +/− 0.0001	3361.751 +/− 29.307	19.834	0.99
Env140-H1[c]	0.0043 +/− 0.0001	586.8043 +/− 13.112	2.523	0.99

[a]Quantification of fluorescence curve shown in Figure 2G.
[b]Quantification of fluorescence curves shown in Figure 3B.
[c]Quantification of fluorescence curves shown in Figure 3D.

such as the tRNA scaffold (20). However, these scaffolds interfere with the ribozyme-split aptamer design, which limits this assay to *in vitro* applications.

SUPPLEMENTARY DATA

Supplementary Data are available at NAR Online.

FUNDING

European Research Council (ERC) advanced (ProNet, 321381); National Centre of Competence in Research (NCCR) Molecular Systems Engineering (in part). Funding for open access charge: ETH Zurich.
Conflict of interest statement. None declared.

REFERENCES

1. Breaker,R.R. and Joyce,G.F. (2014) The expanding view of RNA and DNA function. *Chem. Biol.*, **21**, 1059–1065.
2. Mayer,G. (2009) The chemical biology of aptamers. *Angew. Chem.*, **48**, 2672–2689.
3. Lincoln,T.A. and Joyce,G.F. (2009) Self-sustained replication of an RNA enzyme. *Science*, **323**, 1229–1232.
4. Bhadra,S. and Ellington,A.D. (2014) Design and application of cotranscriptional non-enzymatic RNA circuits and signal transducers. *Nucleic Acids Res.*, **42**, e58.
5. Bhadra,S. and Ellington,A.D. (2014) A Spinach molecular beacon triggered by strand displacement. *RNA*, **20**, 1183–1194.
6. Green,A.A., Silver,P.A., Collins,J.J. and Yin,P. (2014) Toehold switches: de-novo-designed regulators of gene expression. *Cell*, **159**, 925–939.
7. Rodrigo,G., Landrain,T.E. and Jaramillo,A. (2012) De novo automated design of small RNA circuits for engineering synthetic riboregulation in living cells. *Proc.Natl Acad. Sci. U.S.A.*, **109**, 15271–15276.
8. Auslander,D., Wieland,M., Auslander,S., Tigges,M. and Fussenegger,M. (2011) Rational design of a small molecule-responsive intramer controlling transgene expression in mammalian cells. *Nucleic Acids Res.*, **39**, e155.
9. Grabow,W. and Jaeger,L. (2013) RNA modularity for synthetic biology. *F1000prime Reports*, **5**, 46.

10. Saito,H. and Inoue,T. (2009) Synthetic biology with RNA motifs. *Int. J. Biochem. Cell Biol.*, **41**, 398–404.
11. Wittmann,A. and Suess,B. (2012) Engineered riboswitches: expanding researchers' toolbox with synthetic RNA regulators. *FEBS Lett.*, **586**, 2076–2083.
12. Wieland,M. and Hartig,J.S. (2008) Improved aptazyme design and in vivo screening enable riboswitching in bacteria. *Angew. Chem.*, **47**, 2604–2607.
13. Wittmann,A. and Suess,B. (2011) Selection of tetracycline inducible self-cleaving ribozymes as synthetic devices for gene regulation in yeast. *Mol. Biosyst.*, **7**, 2419–2427.
14. Win,M.N. and Smolke,C.D. (2007) A modular and extensible RNA-based gene-regulatory platform for engineering cellular function. *Proc.Natl Acad. Sci. U.S.A.*, **104**, 14283–14288.
15. Auslander,S., Ketzer,P. and Hartig,J.S. (2010) A ligand-dependent hammerhead ribozyme switch for controlling mammalian gene expression. *Mol. Biosyst.*, **6**, 807–814.
16. Khvorova,A., Lescoute,A., Westhof,E. and Jayasena,S.D. (2003) Sequence elements outside the hammerhead ribozyme catalytic core enable intracellular activity. *Nat. Struct. Biol.*, **10**, 708–712.
17. Perreault,J., Weinberg,Z., Roth,A., Popescu,O., Chartrand,P., Ferbeyre,G. and Breaker,R.R. (2011) Identification of hammerhead ribozymes in all domains of life reveals novel structural variations. *PLoS Comput. Biol.*, **7**, e1002031.
18. Arora,A., Sunbul,M. and Jaschke,A. (2015) Dual-colour imaging of RNAs using quencher- and fluorophore-binding aptamers. *Nucleic Acids Res.*, **43**, e144.
19. Paige,J.S., Wu,K.Y. and Jaffrey,S.R. (2011) RNA mimics of green fluorescent protein. *Science*, **333**, 642–646.
20. Strack,R.L. and Jaffrey,S.R. (2015) Live-cell imaging of mammalian RNAs with Spinach2. *Methods Enzymol.*, **550**, 129–146.
21. Akter,F. and Yokobayashi,Y. (2015) RNA signal amplifier circuit with integrated fluorescence output. *ACS Synth. Biol.*, **4**, 655–658.
22. Strack,R.L., Song,W. and Jaffrey,S.R. (2014) Using Spinach-based sensors for fluorescence imaging of intracellular metabolites and proteins in living bacteria. *Nat. Protoc.*, **9**, 146–155.
23. Rogers,T.A., Andrews,G.E., Jaeger,L. and Grabow,W.W. (2015) Fluorescent monitoring of RNA assembly and processing using the split-spinach aptamer. *ACS Synth. Biol.*, **4**, 162–166.
24. Huang,H., Suslov,N.B., Li,N.S., Shelke,S.A., Evans,M.E., Koldobskaya,Y., Rice,P.A. and Piccirilli,J.A. (2014) A G-quadruplex-containing RNA activates fluorescence in a GFP-like fluorophore. *Nat. Chem. Biol.*, **10**, 686–691.
25. Warner,K.D., Chen,M.C., Song,W., Strack,R.L., Thorn,A., Jaffrey,S.R. and Ferre-D'Amare,A.R. (2014) Structural basis for activity of highly efficient RNA mimics of green fluorescent protein. *Nat. Struct. Mol. Biol.*, **21**, 658–663.
26. Hertel,K.J., Pardi,A., Uhlenbeck,O.C., Koizumi,M., Ohtsuka,E., Uesugi,S., Cedergren,R., Eckstein,F., Gerlach,W.L., Hodgson,R. *et al.* (1992) Numbering system for the hammerhead. *Nucleic Acids Res.*, **20**, 3252.
27. Auslander,S., Stucheli,P., Rehm,C., Auslander,D., Hartig,J.S. and Fussenegger,M. (2014) A general design strategy for protein-responsive riboswitches in mammalian cells. *Nat. Methods*, **11**, 1154–1160.
28. McDowell,S.E., Jun,J.M. and Walter,N.G. (2010) Long-range tertiary interactions in single hammerhead ribozymes bias motional sampling toward catalytically active conformations. *RNA*, **16**, 2414–2426.
29. Kennedy,A.B., Liang,J.C. and Smolke,C.D. (2013) A versatile cis-blocking and trans-activation strategy for ribozyme characterization. *Nucleic Acids Res.*, **41**, e41.
30. Roth,A., Weinberg,Z., Chen,A.G., Kim,P.B., Ames,T.D. and Breaker,R.R. (2014) A widespread self-cleaving ribozyme class is revealed by bioinformatics. *Nat. Chem. Biol.*, **10**, 56–60.
31. Zadeh,J.N., Steenberg,C.D., Bois,J.S., Wolfe,B.R., Pierce,M.B., Khan,A.R., Dirks,R.M. and Pierce,N.A. (2011) NUPACK: analysis and design of nucleic acid systems. *J. Comput. Chem.*, **32**, 170–173.